environmental microbiology

Environmental Microbiology (2021) **23**(8), 4214–4227 doi:10.1111/1462-2920.15598

Formate metabolism in the acetogenic bacterium *Acetobacterium woodii*

Jimyung Moon,[1] Judith Dönig,[1] Sina Kramer,[1] Anja Poehlein,[2] Rolf Daniel [2] and Volker Müller [1]*

[1]*Department of Molecular Microbiology & Bioenergetics, Institute of Molecular Biosciences, Johann Wolfgang Goethe University, Max-von-Laue Str. 9, Frankfurt, D-60438, Germany.*

[2]*Göttingen Genomics Laboratory, Institute for Microbiology and Genetics, Georg August University, Grisebachstr. 8, Göttingen, D-37077, Germany.*

Summary

Acetogenic bacteria are already established as biocatalysts for production of high-value compounds from C1 substrates such as $H_2 + CO_2$ or CO. However, little is known about the physiology, biochemistry and bioenergetics of acetogenesis from formate, an interesting feedstock for biorefineries. Here, we analysed formate metabolism in the model acetogen *Acetobacterium woodii*. Cells grew optimally on 200 mM formate to an optical density of 0.6. Formate was exclusively converted to acetate (and CO_2) with a ratio of 4.4:1. Transcriptome analyses revealed genes/enzymes involved in formate metabolism. Strikingly, *A. woodii* has two genes potentially encoding a formyl-THF synthetase, *fhs1* and *fhs2*. *fhs2* forms an operon with a gene encoding a potential formate transporter, *fdhC*. Deletion of *fhs2/fdhC* led to a reduced growth rate, formate consumption and optical densities. Acetogenesis from $H_2 + CO_2$ was accompanied by transient formate production; strikingly, formate reutilization was completely abolished in the *Δfhs2/fdhC* mutant. Take together, our studies gave the first detailed insights into the formatotrophic lifestyle of *A. woodii*.

Abbreviations

OD_{600}	optical density
PCR	polymerase chain reaction
Rnf	Rhodobacter nitrogen fixation
THF	tetrahydrofolate
WLP	Wood-Ljungdahl pathway

Received 25 January, 2021; accepted 12 May, 2021. *For correspondence. E-mail vmueller@bio.uni-frankfurt.de; Tel. (+49) 69 79829507; Fax: (+49) 69 79829306.

Introduction

Acetogenic bacteria are a specialized group of strictly anaerobic bacteria that convert 2 mol of carbon dioxide into acetate *via* the Wood-Ljungdahl Pathway (WLP) (Drake, 1994; Müller, 2003; Ragsdale and Pierce, 2008). The WLP consists of two linear branches, the methyl-branch in which CO_2 is reduced to the methyl group of acetate and the carbonyl branch in which a second molecule of CO_2 is reduced to CO, the precursor of the carbonyl group of acetate. Both branches convey into acetyl-CoA, the precursor of biomass as well as of acetate. The electron donor for the WLP can be hydrogen (Wood *et al*., 1986; Schuchmann and Müller, 2013), allowing for lithotrophic growth, or sugars (Fontaine *et al*., 1942; Balch *et al*., 1977; Leigh *et al*., 1981), alcohols (Buschhorn *et al*., 1989; Bertsch *et al*., 2016) or aldehydes (Daniel *et al*., 1991). In addition, acetogens grow by conversion of other C1 substrates that are fed directly into the WLP such as carbon monoxide (Genthner and Bryant, 1982; Lynd *et al*., 1982; Lorowitz and Bryant, 1984; Savage *et al*., 1987; Daniel *et al*., 1990; Tanner *et al*., 1993; Bertsch and Müller, 2015; Weghoff and Müller, 2016), formaldehyde (Kallen and Jencks, 1966; Schink, 1994), or methyl groups (Kreft and Schink, 1997; Poehlein *et al*., 2012; Kremp *et al*., 2018; Lechtenfeld *et al*., 2018; Kremp and Müller, 2020). To provide the electrons for CO_2 reduction to CO, part of formaldehyde or the methyl groups have to be oxidized to CO_2 by a reversal of the methyl branch of the WLP. Formate is also an intermediate in the WLP and known as a substrate for some acetogens (Balch *et al*., 1977; Leigh *et al*., 1981; Breznak and Switzer, 1986; Traunecker *et al*., 1991; Mechichi *et al*., 1998; Küsel *et al*., 2000; Simankova *et al*., 2000).

Growth of acetogens on C1 compounds is of high biotechnological interest. Some acetogens are already used as biocatalysts for ethanol production from $H_2 + CO_2 +$ CO (synthesis gas). Methanol is another promising feedstock for acetogenic biorefineries, as is formate. Formate

can be produced from carbon dioxide and hydrogen and the acetogens *Acetobacterium woodii* and *Thermoanaerobacter kivui* have highest rates of formate production (Schuchmann and Müller, 2013; Schwarz *et al*., 2018). Formate can also be produced chemically, for example, *via* electrochemical reduction of CO_2 with electricity generated by fossil carbon, biomass or renewable energy (Yishai *et al*., 2016). Formate can then be used as feedstock for various aerobic and anaerobic bacteria and archaea. Surprisingly, little is known about the enzymology of acetogenesis from formate in acetogenic bacteria. To fill this gap is the more important since *A. woodii* has a gene cluster that encodes a second formyl-THF synthetase along with a potential formate transporter. Here, we have addressed the pathway for acetogenesis from formate and the enzymes involved in *A. woodii*.

Results

Growth of A. woodii *on formate*

In order to optimize growth of *A. woodii* on formate, various concentrations of sodium formate were tested as sole carbon source (Fig. 1A). Cells grown under fructose limitation (2.5 mM) were transferred to media containing sodium formate as carbon and energy source. Growth did not start immediately but only after a lag phase of ≈ 6 h. The final OD_{600} increased with increasing formate concentrations and a maximum was reached at 200–300 mM formate. Formate concentrations higher than 300 mM did not lead to higher ODs. The highest growth rate occurred with cells grown on 100 and 200 mM formate, reaching 0.12 h^{-1} (Fig. 1B). Above 300 mM formate, the growth rate decreased drastically, reaching the lowest rate of 0.06 h^{-1} with 500 mM formate. The following experiments were performed with 200 mM formate.

Formate conversion during growth led to acetate formation (Fig. 2). 205.5 mM formate was consumed in 35 h as the growth reached its stationary phase (OD 0.6) and 46.7 mM acetate was produced in 40 h. The ratio of formate:acetate was 4.4:1 with an electron recovery of 91%. The pH of the medium increased from 7.4 to 9.3. To analyse the effect of the initial pH on growth and final yields, growth experiments were performed in medium with low initial pH of 4.5, 5.2, 5.8 and 6.4. Cells did not grow at pH 4.5, 5.2 and 5.8 and at pH 6.4 growth rate and final yield was the same as at pH 7.2 (data not shown). Growth as well as final yield was also not stimulated when the bicarbonate buffer was changed to Tris, glycylglycine, imidazole or PIPES. Therefore, the bicarbonate buffer was used in the following for cultivation.

Transcriptional organization of genes involved in formate uptake and initial metabolism

In the genome of *A. woodii*, there is one formate transporter annotated (Poehlein *et al*., 2012). The putative formate/nitrite transporter gene, *fdhC* (Awo_c08050) is located next to a formyl-THF synthetase encoding gene, *fhs2* (Awo_c08040), in the same direction (Fig. 3A). Formyl-THF synthetase catalyses the conversion of formate to formyl-THF and this has been studied in the thermophilic acetogen *Moorella thermoacetica* (Lovell *et al*., 1990; Radfar *et al*., 2000a,b). Upstream of these

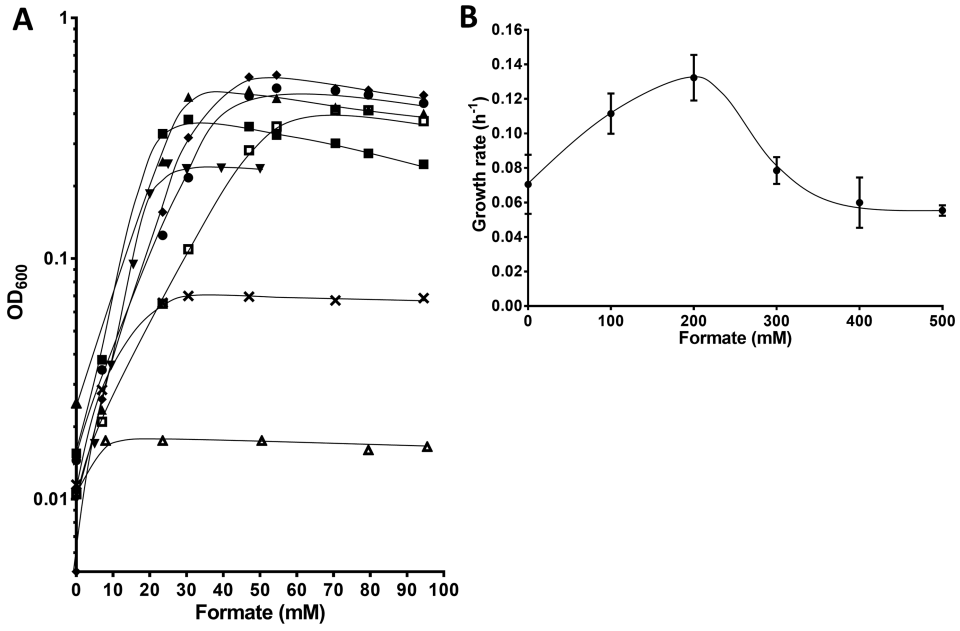

Fig. 1. Growth of *A. woodii* on formate.
A. Dependence of growth of *A. woodii* on the formate concentration. The growth experiments were performed in 5 ml complex medium in the presence of 0 (×), 50 (▼), 100 (■), 200 (▲), 300 (♦), 400 (●), 500 (□) and 1000 mM (Δ) sodium formate as substrate. The pre-culture for inoculation was grown on 100 mM sodium formate. The experiments were performed in biological duplicates and one representative growth curve is shown.
B. Dependence of the growth rate of *A. woodii* on the formate concentration. Data were taken from the experiments depicted in panel A. Each data point indicates a mean with standard error of the mean (SEM).

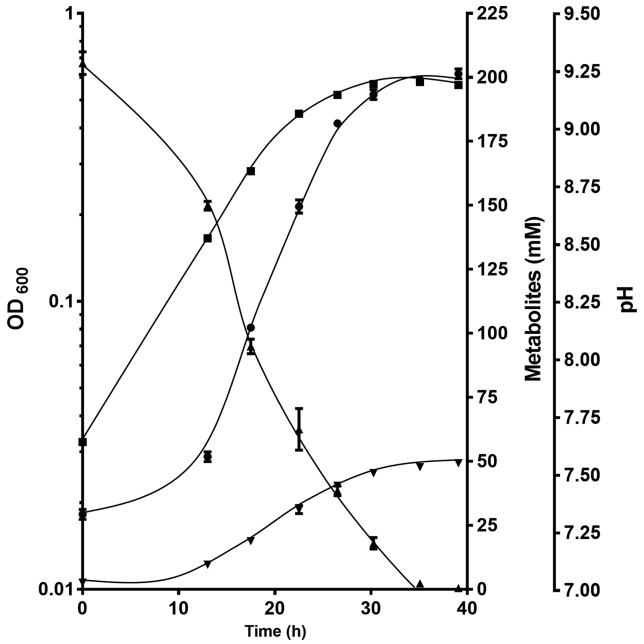

Fig. 2. Formate consumption and acetate formation during growth of *A. woodii*. The growth experiments were performed in 50 ml complex medium in presence of 200 mM sodium formate. Optical densities (■), pH values (●), formate (▲) and acetate (▼) were determined. Each data point indicates a mean ± SEM; $n = 2$ independent experiments.

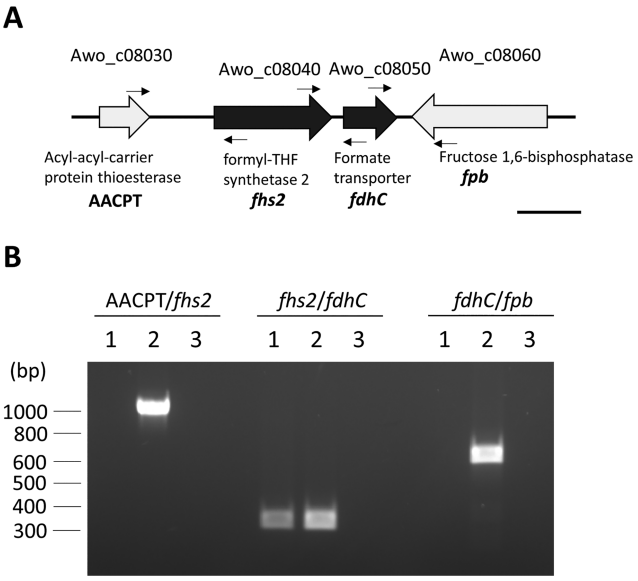

Fig. 3. Genomic arrangement and expression analysis of *fhs2/fdhC* genes in *A. woodii*.
A. Genomic organization of *fhs2/fdhC* genes.
B. Transcriptional organization of *fhs2/fdhC* genes.
For the analysis, total RNA from *A. woodii* was prepared and the contaminating DNA was removed. cDNA was synthesized by reverse transcriptase. To analyse the transcriptional organization, cDNA was used as template for PCR to bridge the intergenic regions of the *fhs2/fdhC* genes (lane 1). Genomic DNA and RNA were used as positive and negative controls respectively (lanes 2, 3). Primers used in this study are described in Materials and Methods and their location is indicated by arrows in panel A.

two genes is an acyl-acyl carrier protein thioesterase encoding gene (Awo_c08030) with the same direction as *fhs2/fdhC*. Downstream is a gene encoding a fructose-1,-6-bisphosphatase (*fpb*, Awo_c08060) in the opposite direction. In addition to *fhs2*, there is another gene, *fhs1* (Awo_c09260) also potentially encoding a formyl-THF synthetase. *fhs1* is part of the gene cluster that encodes methenyl-THF cyclohydrolase (*fchA*, Awo_c09270), methylene-THF dehydrogenase (*folD*, Awo_c09280) and methyl-THF reductase (*RnfC2*, Awo_c09290; *MetV*, Awo_c09300; *MetF*, Awo_c09310), which catalyse the next steps after formyl-THF formation in the methyl-branch of the WLP (Schuchmann and Müller, 2014). Fhs1 and Fhs2 are 98% identical on the amino acid level.

To identify the transcriptional organization of the genes *fhs2* and *fdhC*, mRNA was prepared from cells grown on 200 mM formate in minimal media and harvested in the exponential growth phase (OD_{600} of 0.1). cDNA was synthesized and used as template in a PCR with primers that link the intergenic regions between Awo_c08030 and *fhs2* (Awo_c08040), *fhs2* (Awo_c08040) and *fdhC* (Awo_c08050), and *fdhC* (Awo_c08050) and *fpb* (Awo_c08060) (Fig. 3B). This bridging PCR revealed that *fhs2* and *fdhC* are on one transcript while Awo_c08030 and *fpb* genes are not part of this operon.

Transcriptomic analyses for genes involved in formate metabolism

To identify genes involved in formate metabolism, transcriptome analyses were performed. As observed before, the presence of yeast extract in the growth medium led to the expression of genes involved in the utilization of glycine betaine (GB) (Lechtenfeld *et al*., 2018) or alanine (Dönig and Müller, 2018) as carbon and energy source (Table S1).

In addition, genes involved in flagella formation were upregulated only compared to fructose-grown cells (Table S1). On the other hand, genes involved in riboflavin synthesis, *ribD* (Awo_c00550), *ribE* (Awo_c00560), *ribAB* (Awo_c00570) and *ribH* (Awo_c00580) were the most downregulated genes in fructose-grown cells (Table S2). Moreover, some genes encoding proteins involved in glycolysis such as 1-phosphofructokinase (Awo_c03330; *fruK*), fructose-specific PTS system II components (Awo_c03340), 6-phosphofructokinase (Awo_c12790; *pfkA*), pyruvate kinase (Awo_c12800; *pyk*), triosephosphate isomerase (Awo_c24510; *tpiA2*) and a transcriptional regulator (Awo_c24540) were also downregulated. Twenty genes encoding ribosomal

proteins were downregulated as well. In comparison to $H_2 + CO_2$-grown cells, genes involved in utilization of lactate (Weghoff *et al*., 2015; Schoelmerich *et al*., 2018) were downregulated as well as several genes involved in sugar metabolism (Table S3). Besides, one gene cluster encoding an ABC transport system was highly downregulated during formate metabolism. Overall, the changes in transcript levels were low in general when formate- and fructose- or $H_2 + CO_2$-grown cells were compared.

The transcript counts of *fhs1* (Awo_c09260) and *fhs2* (Awo_c08040) were higher in cells grown on formate than those grown on fructose, with a fold change of 2.0 and 1.2, while counts were slightly lower compared to $H_2 + CO_2$-grown cells (Table 1). *fdhC* (Awo_c08050) levels in formate- and fructose-grown cells compared to fructose were similar, however, *fdhC* was downregulated compared to $H_2 + CO_2$, with a fold change of −1.5. The abundance of HDCR (Awo_c08190 – Awo_c08260) transcripts was higher in cells grown on formate compared to

Table 1. Transcript abundance of genes involved in formate metabolism of *A. woodii*.

			Substrate			Log_2 (fold change)	
Gene	Annotation	Function	fructose	$H_2 + CO_2$	formate	vs. fructose	vs. $H_2 + CO_2$
Awo_c08050	Formate/nitrite transporter FdhC	Formate transport	2263	8055	2809	0.29	−1.46
Awo_c09260	Formyl-THF synthetase Fhs1	Synthesis of formyl-THF	8995	55,885	37,987	2.03	−0.50
Awo_c08040	Formyl-THF synthetase Fhs2		8692	31,756	20,750	1.22	−0.57
Awo_c08190	Formate dehydrogenase FdhF1	HDCR	135	179	124	−0.12	−0.50
Awo_c08200	Hydrogenase, Fe-S subunit HycB1		33	38	31	−0.09	−0.25
Awo_c08210	Formate dehydrogenase FdhF2		11,894	23,890	38,245	1.67	0.66
Awo_c08230	Hydrogenase, Fe-S subunit HycB2		1297	2545	4571	1.77	0.79
Awo_c08240	Formate dehydrogenase accessory protein FdhD		846	1278	1526	0.82	0.24
Awo_c08250	Hydrogenase, Fe-S subunit HycB3		819	1488	1529	0.88	0.04
Awo_c08260	Iron hydrogenase HydA2		3070	5468	8080	1.37	0.55
Awo_c09270	Methenyltetrahydrofolate cyclohydrolase FchA	WLP methyl branch	1748	9652	5786	1.65	−0.65
Awo_c09280	Methylenetetrahydrofolate dehydrogenase FolD	WLP methyl branch	3748	23,970	9742	1.32	−1.23
Awo_c09290	Electron transport complex Rnf, C subunit RnfC2	MTHFR (WLP methyl branch)	11,239	70,294	37,319	1.66	−0.82
Awo_c09300	5,10-Methylenetetrahydrofolate reductase SSU MetV		2343	14,410	8544	1.79	−0.66
Awo_c09310	5,10-Methylenetetrahydrofolate reductase LSU MetF		6395	38,668	19,554	1.54	−0.90
Awo_c10670	CODH Ni^{2+}-insertion accessory protein CooC1	CODH/ACS	1622	3377	2327	0.51	0.52
Awo_c10680	Corrinoid activation/regeneration protein		5006	12,369	15,752	1.63	0.33
Awo_c10690	Hypothetical protein		1136	2843	3324	1.53	0.22
Awo_c10700	Hypothetical protein		881	2093	4958	2.41	1.11
Awo_c10710	CFeS protein, SSU AcsD		19,598	96,011	44,249	1.12	−1.06
Awo_c10720	CFeS protein, LSU AcsC		22,057	116,013	72,258	1.68	−0.65
Awo_c10730	Methyltransferase 2		17,381	77,637	58,026	1.71	−0.40
Awo_c10740	CODH, catalytic subunit AcsA		12,486	74,496	83,195	2.71	0.15
Awo_c10750	CODH Ni^{2+}-insertion accessory protein CooC2		2712	17,121	24,461	3.14	0.47
Awo_c10760	ACS, catalytic subunit AcsB		16,548	108,808	101,503	2.60	−0.10
Awo_c19620	Phosphotransacetylase Pta	Acetate formation	664	688	482	−0.45	−0.49
Awo_c21260	Acetate kinase AckA		5215	7093	2700	−0.92	−1.36
Awo_c22010	Electron transport complex protein RnfB	RnF complex	3523	9548	6781	0.91	−0.47
Awo_c22020	Electron transport complex protein RnfA		983	2846	2541	1.29	−0.14
Awo_c22030	Electron transport complex protein RnfE		1153	3051	2494	1.05	−0.26
Awo_c22040	Electron transport complex protein RnfG		1362	4068	4442	1.67	0.12
Awo_c22050	Electron transport complex protein RnfD		2235	5437	3547	0.64	−0.57
Awo_c22060	Electron transport complex protein RnfC1		4300	10,443	6212	0.51	−0.72
Awo_c26970	Iron hydrogenase HydA1	Bifurcating hydrogenase	18,113	75,732	77,622	2.05	0.03
Awo_c26980	Iron hydrogenase HydB		15,588	61,188	57,341	1.81	−0.08
Awo_c26990	Iron hydrogenase HydD		2360	9020	8119	1.75	−0.14
Awo_c27000	Sensory transduction histidine kinase HydE		3352	11,277	13,985	2.01	0.29

(Continues)

Table 1. Continued

Gene	Annotation	Function	Substrate			Log_2 (fold change)	
			fructose	$H_2 + CO_2$	formate	vs. fructose	vs. $H_2 + CO_2$
Awo_c27010	Iron hydrogenase HydC		2760	9690	4900	0.79	−0.93
Awo_c02140	ATP synthase protein I AtpI	ATP synthase	1569	3929	3327	1.01	−0.21
Awo_c02150	F-type ATP synthase subunit A AtpB		5581	14,888	6510	0.21	−1.10
Awo_c02160	F-type ATP synthase subunit E AtpE1		2272	5816	3442	0.52	−0.65
Awo_c02170	F-type ATP synthase subunit E AtpE2		527	1443	897	0.66	−0.56
Awo_c02180	F-type ATP synthase subunit E AtpE3		706	1822	1053	0.54	−0.73
Awo_c02190	F-type ATP synthase subunit F AtpF		4331	9943	3834	−0.15	−1.28
Awo_c02200	F-type ATP synthase subunit H AtpH		2582	5893	4311	0.67	−0.39
Awo_c02210	F-type ATP synthase subunit A AtpA		18,460	46,259	21,599	0.21	−1.05
Awo_c02220	F-type ATP synthase subunit G AtpG		7575	19,704	11,129	0.51	−0.74
Awo_c02230	F-type ATP synthase subunit D AtpD		16,026	47,960	28,436	0.76	−0.67
Awo_c02240	F-type ATP synthase subunit C AtpC		2932	7816	9495	1.65	0.25
Awo_c09930	Na^+/H^+ antiporter NhaP	Na^+ transport	622	329	286	−0.98	−0.16
Awo_c15580	Sodium/hydrogen exchanger		538	420	219	−1.25	−0.88
Awo_c20250	K^+-dependent Na^+/Ca^+ exchanger		64	47	58	−0.12	0.28
Awo_c24490	Membrane-bound sodium-translocating pyrophosphatase HppA		10,997	11,464	3127	−1.79	−1.84
Awo_c05870	Carbonic anhydrase CynT	pH regulation CO_2 capture	836	936	941	0.17	0.01
Awo_c08610	Arginine deiminase ArgA	Acid tolerance	476	457	332	−0.51	−0.45
Awo_c08620	Ornithine carbamoyltransferase ArgF1		817	761	398	−1.02	−0.91
Awo_c12250	Ornithine carbamoyltransferase ArgF2		871	509	623	−0.44	0.26
Awo_c12270	Carbamate kinase ArcC		402	232	566	0.47	1.26
Awo_c09320	Dihydrolipoamide dehydrogenase LpdA1	Glycine synthase	878	1894	695	−0.32	−1.41
Awo_c09330	Glycine cleavage system H protein GcvH1		278	499	210	−0.37	−1.19
Awo_c12540	Dihydrolipoamide dehydrogenase LpdA2		96	84	163	0.71	0.89
Awo_c22560	Glycine cleavage system H protein GcvH2		396	593	639	0.66	0.11
Awo_c32780	Glycine dehydrogenase subunit 2 GcvPB		3203	4320	10,220	1.63	1.19
Awo_c32790	Glycine dehydrogenase subunit 1 GcvPA		2966	4618	11,376	1.88	1.23
Awo_c32800	Aminomethyltransferase GcvT		5814	6540	12,124	1.00	0.83
Awo_c32810	Glycine cleavage system H protein GcvH3		734	764	1229	0.69	0.62
Awo_c24330	Pyruvate:ferredoxin oxidoreductase NifJ	Pyruvate formation/ oxidation	15,453	14,343	51,682	1.68	1.78
Awo_c06200	Pyruvate:ferredoxin oxidoreductase, beta subunit PorB		361	394	962	1.36	1.22
Awo_c06210	Pyruvate:ferredoxin oxidoreductase, alpha subunit PorA		1177	942	2888	1.26	1.58
Awo_c14910	Pyruvate formate lyase activating enzyme PflA		14	26	99	2.76	1.84
Awo_c14920	Pyruvate formate lyase PflB1		33	61	378	3.45	2.59
Awo_c14930	Pyruvate formate lyase PflB2		16	42	93	2.49	1.08
Awo_c14940	Pyruvate formate lyase activating enzyme PflA		2	15	35	3.60	1.04
Awo_c14960	Pyruvate formate lyase PflB3		32	56	125	1.91	1.06

fructose and $H_2 + CO_2$, except *fdhF1* and *HycB1*. On the other hand, other genes encoding WLP enzymes in the methyl branch such as *fchA*, *folD*, *rnfC2*, *metV* and *metF* were upregulated compared to fructose-grown cells, while these were downregulated compared to $H_2 + CO_2$-grown cells. The levels of genes encoding CODH/ACS in formate-grown cells was higher than in fructose-grown cells, but similar to $H_2 + CO_2$-grown cells. The genes encoding enzymes involved in acetate formation from acetyl-CoA such as phosphotransacetylase (Awo_c19620; *pta*) and acetate kinase (Awo_c21260; *ackA*) were downregulated during growth on formate. Gene clusters encoding the energy-conserving Rnf complex, the ATP synthase and the electron bifurcating hydrogenase (Schuchmann and Müller, 2014) were upregulated in formate-grown cells compared to fructose-grown cells, but were downregulated compared to $H_2 + CO_2$-grown cells. The sodium salt of formate was used as a substrate, but the genes potentially involved in Na^+ homeostasis were downregulated. The gene encoding carbonic anhydrase (Awo_c05870; *cynT*) was similarly expressed with all substrates.

In addition to the WLP, glycine synthase pathway is a possible CO_2-fixing metabolic pathway. Among acetogens, it has been reported that *Clostridium drakei* has a functional glycine synthase as well as glycine reductase pathway (Song *et al*., 2020). *A. woodii* possesses genes encoding all four proteins involved in the glycine synthase pathway,

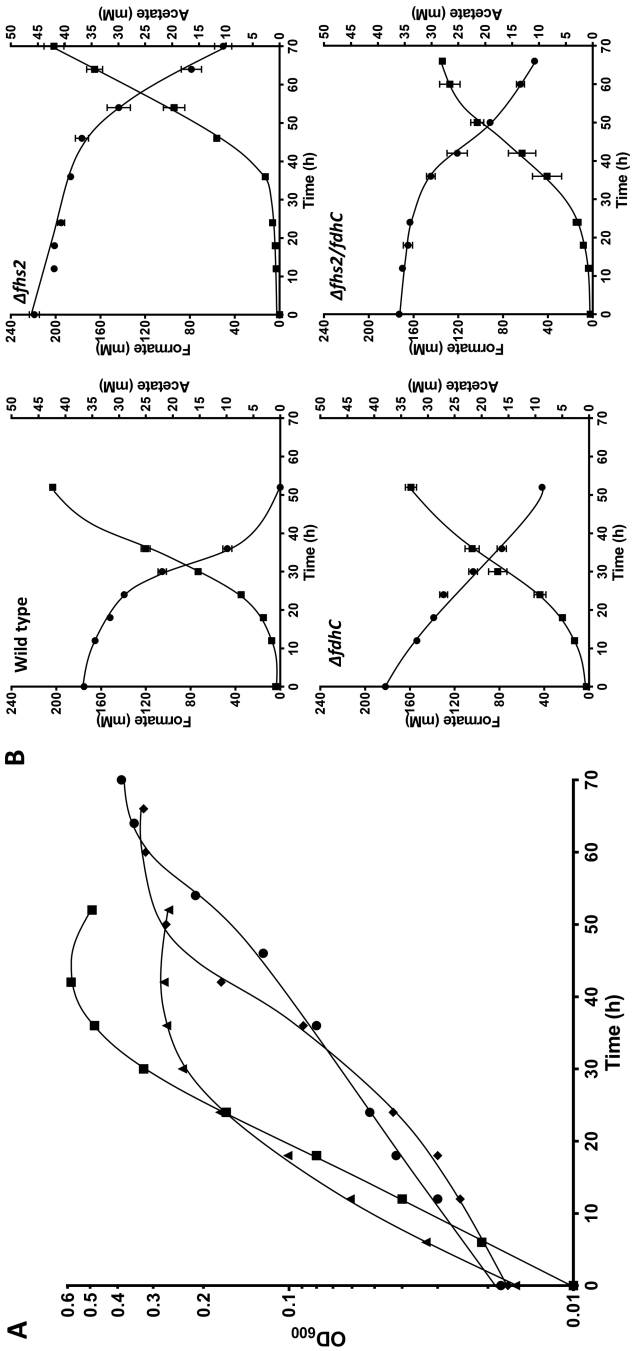

Fig. 4. Formate consumption and acetate formation during growth of *A. woodii* wild type and mutants on formate.
A. Growth of *A. woodii* wild type and mutants on formate. Cells of the wild type (■), *Δfhs2* (●), *ΔfdhC* (▲) and *Δfhs2/fdhC* (◆) were inoculated from formate-grown pre-cultures into 50 ml complex medium containing 200 mM sodium formate. The growth experiments were performed in biological triplicates and one representative growth curve is presented.
B. Formate (●) and acetate (■) from the growth experiments of the wild type and mutants were determined by HPLC. Each data point indicates a mean ± SEM; $n = 3$ independent experiments.

but not in one cluster: three genes encoding H protein (*gcvH1*, Awo_c09330; *gcvH2*, Awo_c22560; *gcvH3*, Awo_c32810), two genes encoding dihydrolipoamide dehydrogenase (*lpdA1*, Awo_c09320; *lpdA2*, Awo_c12540), one gene encoding aminomethyltransferase (*gcvT*, Awo_c32800) and two genes encoding glycine dehydrogenase (*gcvPB*, Awo_c32780; *gcvPA*, Awo_c32790). Except *lpdA1* and *gcvH1*, all genes for the glycine synthase pathway were slightly upregulated during formate metabolism, especially a potential gene cluster, Awo_c32780 - Awo_32810. *A. woodii* does not have genes encoding a glycine reductase.

During growth on formate, pyruvate must be generated as it serves as a precursor for various biosynthetic reactions. *A. woodii* possesses genes encoding pyruvate:ferredoxin oxidoreductase (PFOR) as well as pyruvate formate lyase (PFL). PFOR catalyses the oxidation of pyruvate to acetyl-CoA and CO_2 with the concomitant reduction of ferredoxin (Chabriere *et al*., 1999). Awo_c24330 (*nifJ*) was strongly transcribed during growth on formate compared to cells grown on fructose or $H_2 + CO_2$. Awo_c06200 (*porB*) and Awo_c06210 (*porA*) were upregulated, but transcript counts were much lower compared to those of *nifJ*. PFL catalyses the conversion of pyruvate to acetyl-CoA and formate and *vice versa* (Zelcbuch *et al*., 2016). All genes encoding for PFL were expressed stronger in formate grown cells, but total transcript counts were extremely low.

Generation and characterization of deletion mutants

To characterize their role in formate metabolism, the genes *fhs2*, *fdhC* and *fhs2/fdhC* were deleted using the genetic system and the *ΔpyrE* deletion strain of *A. woodii* described before (Westphal *et al*., 2018). For generation of the mutants *Δfhs2*, *ΔfdhC* and *Δfhs2/fdhC*, suicide plasmids pMTL84151_JM_dfhs2, pMTL_84151_SK_dfdhC and pMTL84151_SK_dfhs2/fdhC were constructed, carrying each 500 to 1000 bp of upstream and downstream flanking regions (UFR and DFR) of the respective gene leaving 3 bp behind the start codon and 3 bp in front of stop codon. The promoter region aimed to be remained in the chromosome. Moreover, the plasmids contained *pyrE* gene from *Clostridium acetobutylicum* (Westphal *et al*., 2018) and the chloramphenicol/thiamphenicol resistance cassette (*catP*) from *Clostridium perfringens* (Werner *et al*., 1977) together with its own promoter. For the first selection, the plasmids were integrated into the chromosome at one flanking region under antibiotic pressure with thiamphenicol. Subsequently, disintegration was forced by counter-selection with 5-fluoroorotate since the presence of *pyrE* cassette in the integrated plasmid enabled production of 5-fluorouracil which is toxic to the cells.

The *ΔfdhC* mutant had a slightly reduced growth rate compared to the wild type but the final OD_{600} was reduced by 55% (Fig. 4A). At the same time, formate consumption as well as acetate formation was reduced (Fig. 4B). The *Δfhs2* mutant as well as *Δfhs2/fdhC* double mutant had a more severe growth effect with an extended lag phase; at the same time, formate consumption as well as acetate formation had a lag phase.

In order to study how the deletion of the formate transporter affects growth on different concentration of formate, cells were grown with 20 to 500 mM of formate as substrate. With 20 mM formate, the wild type and the *ΔfdhC* mutant showed similar maximum OD_{600} (0.15) and growth rate (0.07 h^{-1}) (Fig. S2). However, with increasing formate concentrations, the growth rate and the final OD_{600} of the *ΔfdhC* mutant decreased and the difference to the wild type stayed almost constant up to 500 mM formate tested.

Cell suspension experiments

To compare H_2 or acetate production by the mutants, resting cells of the wild type and the mutants were prepared, as described in Material and Methods. When high concentration of sodium formate (350 mM) was given to the wild type and the *Δfhs2/fdhC* mutant, both strains metabolized formate with production of 19 mM acetate and 100 mM H_2 in carbonate-free imidazole buffer or 35 mM acetate and 18 mM H_2 in carbonate-containing imidazole buffer, respectively. In the presence of low concentrations of sodium formate (4 mM) in carbonate-containing imidazole buffer, the *Δfhs2/fdhC* mutant was impaired in formate utilization and acetate production. H_2 production was very low and more or less identical in both strains (Fig. 5). When the experiments were performed in the absence of bicarbonate and CO_2, the wild type as well as the mutant produced much more hydrogen, up to $\approx$ 3 mM, and less acetate (Fig. S3). Again, formate utilization and acetate production was reduced in the *Δfhs2/fdhC* mutant.

Since the formyl-THF synthetase is also involved in acetogenesis from $H_2 + CO_2$, we compared acetate formation from $H_2 + CO_2$ in resting cells of the wild type and the *Δfhs2/fdhC* mutant. The *Δfhs2/fdhC* mutant produced less acetate from $H_2 + CO_2$ (Fig. 6). Acetate formation from $H_2 + CO_2$ was described to be accompanied with a transient production of formate (Peters *et al*., 1999; Oswald *et al*., 2018). This was also observed here. However, the double mutant accumulated around thrice the amount and accumulation was not transient but formate remained at a high level. This phenomenon was also seen with different concentrations of H_2.

Discussion

Here, we have investigated growth of *A. woodii* on formate and acetogenesis from formate as well as the genes

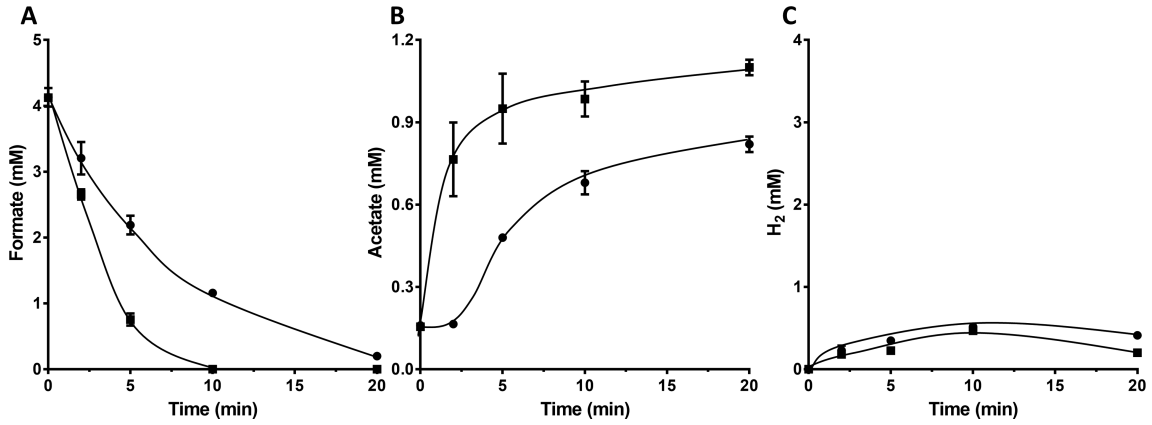

Fig. 5. Formate uptake and conversion into acetate and H_2 by resting cells of *A. woodii* wild type and *Δfhs2/fdhC*. Cells were grown on 20 mM fructose and harvested in late exponential phase. After washing twice, the cells were resuspended in 10 ml imidazole buffer (50 mM imidazole, 20 mM NaCl, 20 mM KCl, 20 mM $MgSO_4$, 60 mM $KHCO_3$, pH 7.0) in 120 ml serum flasks under a N_2/CO_2 atmosphere. 4 mM of sodium formate was given to cell suspension of the wild type (■) and the *Δfhs2/fdhC* mutant (●). Formate (A) and acetate (B) were determined by HPLC. (C) H_2 was determined by gas chromatography and presented as mmol l^{-1} cell suspension. Each data point indicates a mean ± SEM; n = 2 independent experiments.

encoding enzymes involved in formate metabolism. Formate is the first intermediate of the methyl branch of the WLP and was reported to be used as carbon source in *A. woodii* already in 1977 (Balch *et al*., 1977) as well as other acetogens such as *Eubacterium limosum* (Genthner and Bryant, 1987), *Acetobacterium carbolinicus* (Eichler and Schink, 1984) or *Clostridium ljungdahlii* (Tanner *et al*., 1993).

The first step in formate metabolism is its uptake. At the optimal concentration of 200 mM and pH 7.0 ($pKa_{formic\ acid} = 3.75$), 0.1 mM of the substrate was in the form of formic acid, 199.9 mM as formate. Formic acid can diffuse across membranes (Falke *et al*., 2010) and thus, there is no essential need for a transport system. The hallmark of active transport is not only to increase the uptake rate but, more important, to accumulate the substrate inside the cell, at the expense of ATP hydrolysis or the electrochemical ion gradient across the membrane. However, FdhC of *A. woodii* is similar to FocA of *E. coli*, a presumptive channel that facilitates diffusion but does not accumulate but only equilibrate formate concentration outside and inside the cell (Hunger *et al*., 2014; Wiechert and Beitz, 2017). The high concentration of formate required for optimal growth may reflect its uptake by diffusion or facilitated diffusion of formic acid. However, with an alkalinization of the external pH (at a constant internal pH), formic acid will be dragged out of the cells, arguing for active transport of formate. Anyway, the experiments described here demonstrate that FdhC is not essential for growth on the formate concentration tested; however, the presence of FdhC leads to higher final optical densities and lower growth rates. This gives a clear fitness advantage to the cells.

The pathway of acetogenesis from formate has been postulated on theoretical grounds. Four mol of formate enter the WLP, then 3 mol of formate are oxidized to CO_2 to provide the electrons for the reduction of another mol of formate plus 1 mol of CO_2 to acetate *via* the WLP. A key enzyme in formate metabolism is the formate dehydrogenase (FDH) that has been studied in several species. The thermophilic acetogen *M. thermoacetica* has a tungsten-selenium-containing, NADP-specific FDH (Andreesen and Ljungdahl, 1973; Yamamoto *et al*., 1983; Deaton *et al*., 1987). In *Clostridium aciduriri*, the reduction of CO_2 to formate is catalysed by an electron bifurcating FDH (Wang *et al*., 2013). *A. woodii* (Schuchmann and Müller, 2013) and the thermophilic acetogen *Thermoanaerobacter kivui* (Schwarz *et al*., 2018) have a hydrogen-dependent CO_2 reductase (HDCR) in which a formate dehydrogenase module is connected *via* two electron-transferring subunits to a Fe-Fe hydrogenase module. Overall, the genes coding for enzymes of the WLP during growth on formate are upregulated compared to growth on fructose, but slightly downregulated compared to growth on $H_2 + CO_2$. Interestingly, *A. woodii* has a second gene (*fhs2*) encoding a formyl-THF synthetase. *fhs2* builds an operon with *fdhC* encoding the putative formate transporter. A similar genetic arrangement was not found in other acetogens. *T. kivui* has *fhs1* (TKV_c19930) and *fdhC* (TKV_19940) in the same order with an intergenic region of 842 bp (Hess *et al*., 2014), however, it is located in a cluster with other genes for the methyl branch of the WLP. During formate metabolism *fhs2* and *fdhC* as well as *fhs1* together with the genes involved in the methyl branch of the WLP were upregulated compared to fructose-grown cells but slightly downregulated compared to $H_2 + CO_2$-grown cells. Overall, the fold change was low. As *fhs2* and *fdhC* are transcribed in a single transcriptional unit apart from the

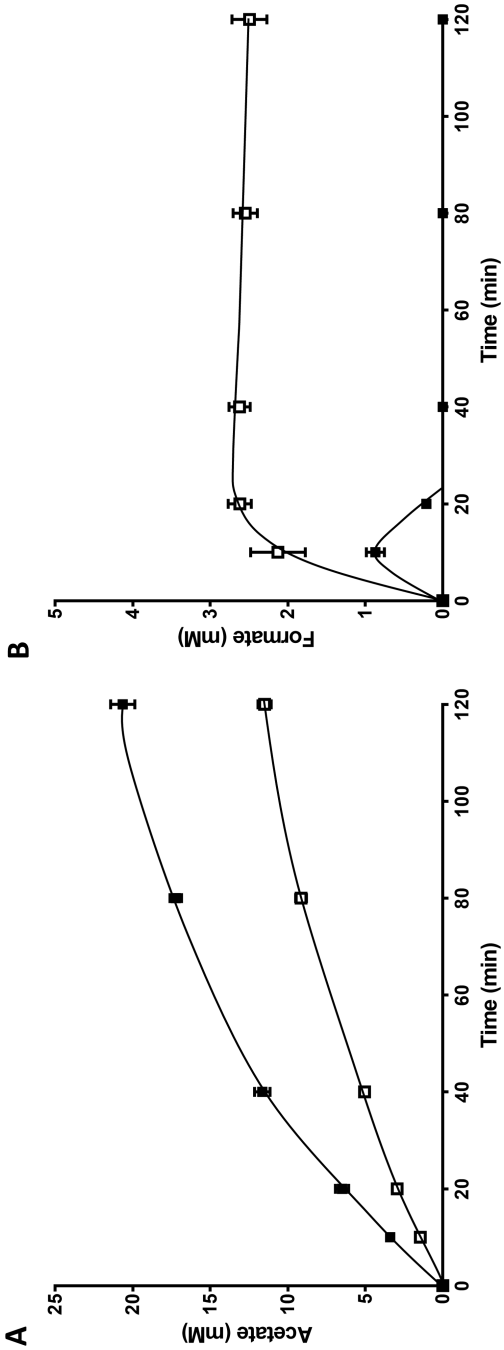

Fig. 6. Conversion of $H_2 + CO_2$ into formate and acetate by resting cells of *A. woodii*. The cells were prepared as described in Fig. 5 and resuspended in 10 ml imidazole buffer (50 mM imidazole, 20 mM NaCl, 20 mM KCl, 20 mM $MgSO_4$, pH 7.0) in 120 ml serum flasks under a N_2 atmosphere. $H_2 + CO_2$ (80:20; vol/vol, 1 bar overpressure) was used as substrate for the wild type (■) or the *Δfhs2/fdhC* mutant (□). Acetate (A) and formate (B) were determined by HPLC. Each data point indicates a mean ± SEM; $n = 2$ independent experiments.

genes for the methyl branch of the WLP, we expected that expression of this transcriptional unit enhances the formate metabolism in *A. woodii*. Indeed, the deletion mutants *Δfhs2* and *Δfhs2/fdhC* showed impaired growth and reduced formate consumption compared to the wild type.

When $H_2 + CO_2$ was given as substrate, formate was transiently accumulated and immediately reutilized in the wild type under carbonate-free condition. The same was observed before (Peters *et al*., 1999; Oswald *et al*., 2018). However, the *Δfhs2/fdhC* mutant could not reutilize formate, instead, formate accumulated to 2.6 mM. From all these observations, we conclude that Fhs2 and FdhC play an important role for initial formate uptake and conversion to formyl-THF especially in the presence of low formate concentrations.

From the physiological, genetic and biochemical data presented we propose that formate is metabolized according to the following equation:

$$HCOOH + 0.3\,ADP + 0.3\,P_i \rightarrow CH_3COOH + 2CO_2 + 2H_2O + 0.3\,ATP$$

as depicted in Fig. 7. This is also supported by an observed Na^+ dependence of acetogenesis from formate and the essential requirement of the Rnf complex for acetate formation from formate (data not shown). A possible bypass of carbon through a potential glycine synthase as in *C. drakei* (Song *et al*., 2020) is not supported by the data.

How biomass is built during growth on formate would be a remaining question. Pyruvate, a precursor for many biosynthetic processes, can be generated by carboxylation of acetyl-CoA, generated *via* the WLP. Pyruvate synthesis *via* PFL would be advantageous during formate metabolism since formate is an educt in the reaction and the reaction is thermodynamically and kinetically independent of external CO_2 concentration in the environment. We observed in the transcriptome analysis that genes encoding PFOR, *porB*, *porA* and *nifJ* are slightly upregulated during growth on formate. The genes *pflA*, *pflB1*, *pflB2*, *pflB3* and *pflC* were upregulated but the overall transcript level was low. Thus, we assume that PFOR is mainly responsible for pyruvate synthesis during formate metabolism. However, which PFOR is responsible for the reaction and why *A. woodii* possesses three *pfl* genes are the remaining questions for further research.

Experimental procedures

Organisms and cultivation

A. woodii strains were routinely cultivated under anaerobic condition at 30°C in the complex medium described

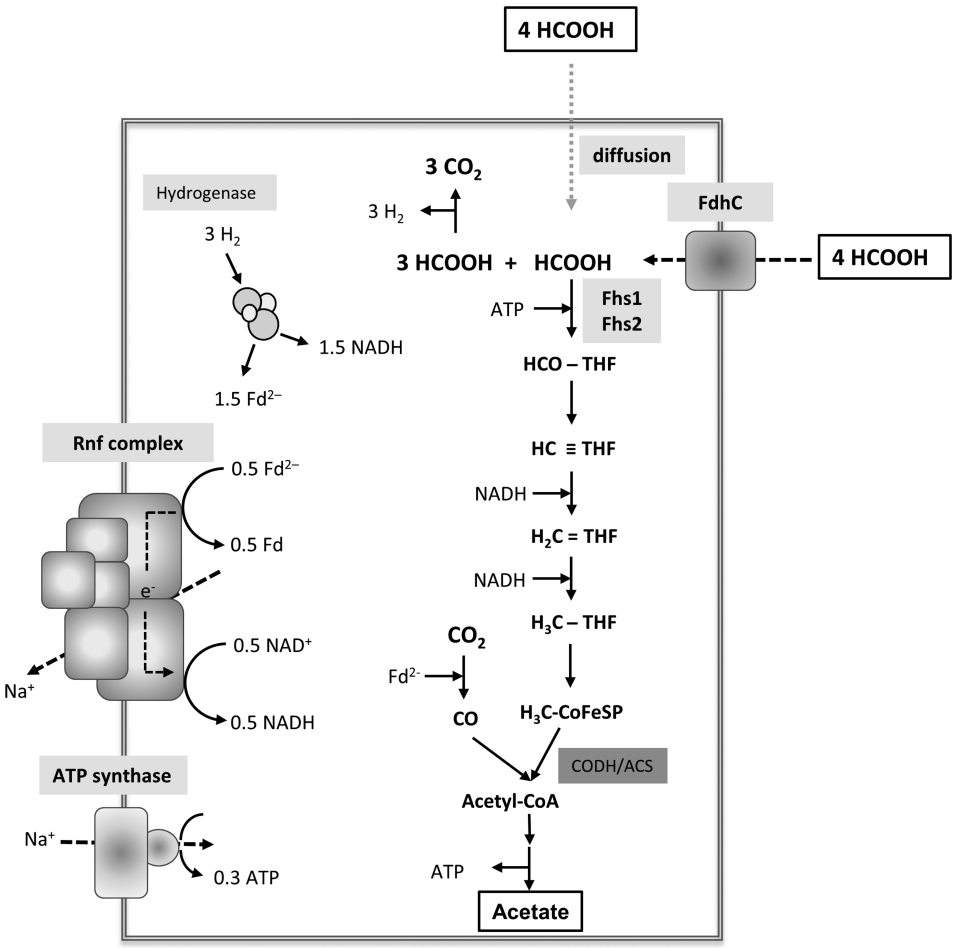

Fig. 7. Acetogenesis from formate in *A. woodii*. Formate is imported *via* the formate transporter (FdhC) or by diffusion. Three mol formate are oxidized to 3 mol CO_2 and 3 mol H_2 by HDCR and 1 mol formate is converted to formyl-THF *via* formyl-THF synthetase (Fhs1/Fhs2). Formyl-THF is further reduced to methyl-THF. One mol CO_2 is reduced to CO and combined with the methyl group by the CODH/ACS complex, generating acetyl-CoA. Acetyl-CoA is further converted to acetate. Balancing of reducing equivalents is achieved by action of the bifurcating hydrogenase (HydABC) and the Rnf complex. The ATP synthase has a Na^+/ATP stoichiometry of 3.66 (Matthies *et al*., 2014), the Na^+/e^- stoichiometry of the Rnf complex is assumed to be 1 Na^+/e^-, based on theoretical consideration (Schuchmann and Müller, 2014).

previously (Heise *et al*., 1989). The *A. woodii* strains used in this study are listed in Table S4. As substrates for growth, 20 mM fructose, 60 mM methanol, 1 bar of $H_2 + CO_2$ (80:20, vol/vol) and various concentrations of sodium formate were used. *E. coli* DH5α and BL21 (DE3) strains were cultivated aerobically at 37°C in LB medium either in presence of chloramphenicol (30 ng μl^{-1}) or ampicillin (100 ng μl^{-1}). Growth was monitored by measuring the optical density at 600 nm (OD_{600}).

Analysis of fhs2/fdhC *gene cluster*

Cells of *A. woodii* grown on 200 mM fructose were harvested in the exponential growth phase. Preparation of RNA and cDNA was performed as described previously (Dönig and Müller, 2018). The prepared cDNA was used as the template for analysing the transcriptional organization of *fhs2/fdhC* genes *via* PCR. For amplification of the intergenic region between Awo_c08030 and Awo_c08040, oligonucleotides AAC_Fhs2_for (5′-ATAAGGCGCAGTGT TTTTATGG-3′) and AAC_Fhs2_rev (5′-CTTGTGCAATTT CAATGTCTGATTTA-3′) were used as primers. For amplification of the intergenic region between Awo_c08040 and Awo_08050, Fhs2_FdhC_for (5′-CTTCCTAAAGTTCCG GCAGC-3′) and Fhs2_FdhC_rev (5′-AAACCATATGCCC CGAAACC-3′) were used. For amplification of the intergenic region between Awo_c08050 and Awo_c08060, FdhC_Fpb_for (5′- CAATCTGGTTTCCGATTATGC-3′) and FdhC_Fpb_rev (5′- GCAACGTCTGGAGAAAGCC-3′) were used. As a positive control, chromosomal DNA of *A. woodii* was used, and as a negative control, the isolated RNA was used.

Transcriptome analyses

For transcriptome analyses, cells were grown on 100 mM sodium formate and harvested in the early exponential growth phase with OD_{600} of 0.1. Harvested cells were resuspended in 800 µl of RLT buffer of the RNeasy Mini Kit (Qiagen, Hilden, Germany) with β-mercaptoethanol (10 $\mu l\ ml^{-1}$), and cell lysis was performed using a

laboratory ball mill. Subsequently, 400 µl of RLT buffer (RNeasy Mini Kit) with β-mercaptoethanol (10 µl ml^{-1}) and 1200 µl of 96% [v/v] ethanol were added. For RNA isolation, the RNeasy Mini Kit was used as recommended by the manufacturer, but instead of RW1 buffer RWT buffer (Qiagen, Hilden, Germany) was used to also isolate RNAs smaller than 200 nt. To determine the RNA integrity number (RIN), the isolated RNA was run on an Agilent Bioanalyzer 2100 using an Agilent RNA 6000 Nano Kit as recommended by the manufacturer (Agilent Technologies, Waldbronn, Germany). Remaining genomic DNA was removed by treatment of the samples with TURBO DNase (ThermoFisher Scientific, Waltham, MA, USA). The RiboZero kit (Illumina Inc., San Diego, CA, USA) was used to reduce the amount of rRNA-derived sequences. For sequencing, the strand-specific cDNA libraries were constructed with a NEBNext Ultra directional RNA library preparation kit for Illumina (New England BioLabs, Frankfurt am Main, Germany) using 100 ng rRNA depleted RNA and 12 PCR cycles. To assess the quality and size of the libraries, samples were run on an Agilent Bioanalyzer 2100 using an Agilent High Sensitivity DNA kit as recommended by the manufacturer (Agilent Technologies, Waldbronn, Germany). The concentration of the libraries was determined using the Qubit® dsDNA HS Assay kit as recommended by the manufacturer (Life Technologies GmbH, Darmstadt, Germany). Sequencing was performed by using the MiSeq instrument (Illumina Inc., San Diego, CA, USA) using the MiSeq reagent kit v3 (150 cycles) for sequencing in the paired-end mode and running 2 × 75 cycles. Fructose-grown cells were used as reference dataset (Kremp *et al*., 2018). Normalization of the reads was done with DeSeq2 (v 1.28.1) (Love *et al*., 2014) and foldchange-shrinkages were calculated with DeSeq2 and the apeglm package (v 1.10.0) (Zhu *et al*., 2019). For analysis based on KEGG annotation, the clusterProfiler (v 3.16.0) (Yu *et al*., 2012) and pathview (v 1.28.0) (Luo and Brouwer, 2013) packages were used. Genes with a $\log_2$-fold change (FC) of +2/−2 and a *p*-adjust value < 0.05 were considered differentially expressed. The sequence data have been submitted to the SRA database.

Generation of A. woodii *Δfhs2, ΔfdhC and Δfhs2/fdhC strains*

The plasmids pMTL84151_JM_dfhs2, pMTL84151_SK_dfdhC and pMTL84151_SK_dfhs2/fdhC were constructed in *E. coli* DH5α (New England Biolabs, Frankfurt am Main, Germany) and transformed into *A. woodii* ΔpyrE strain, as previously described (Westphal *et al*., 2018). These plasmids originated from pMTL84151 (Heap *et al*., 2009) and modified as suicide plasmid which does not possess a Gram positive replicon. In pMTL84151_JM_dfhs2, 1000 bp of upstream- and downstream flanking regions (UFR and DFR) of *fhs2* (Awo_c08040) were cloned into the multiple cloning sites, whereas pMTL84151_SK_dfdhC and pMTL84151_SK_dfhs2/fdhC possess 500 bp of UFR and DFR of *fdhC* (Awo_c08050) or UFR of *fhs2* and DFR of *fdhC*, respectively. Since these plasmids contain a *catP* marker for chloramphenicol/thiamphenicol resistance from *Clostridium perfringens* (Werner *et al*., 1977) and a heterologous *pyrE* from *Clostridium acetobutylicum* (Westphal *et al*., 2018) as a counter selectable marker, the first selection was carried out in an agar plate with complex medium supplemented with 20 mM fructose and 30 ng µl^{-1} thiamphenicol after transformation of plasmids into *A. woodii ΔpyrE* strain by electroporation (625 V, 25 µF, 600 Ω, in 1 mm cuvettes). Then, the thiamphenicol-resistant colonies were further plated onto an agar plate with minimal medium (Westphal *et al*., 2018) supplemented with 20 mM fructose, 1 µg ml^{-1} uracil and 1 mg ml^{-1} 5-FOA to select the cells in which single crossover integrants had been removed and the plasmid had been lost. The deleted region was analysed by PCR with oligonucleotides which bind in front of UFR and behind DFR of the respective gene: aus_fhs2_for (5′-CGCTTCTTGGATATTGATTTCAATC-3′) and aus_fhs2_rev (5′-AATCAGGTCGAAGATCTGGA-3′) for *Δfhs2*, aus_fdhC_for (5′-CGAATACTGCTACGATCTG-3′) and aus_fdhC_rev (5′- GTGTTGATCCCGAAGAAGG-3′) for *ΔfdhC*, aus_ff_for (5′-CCCGAGCAAAGATTGTTTG-3′) and aus_fdhC_rev for *Δfhs2/fdhC*, respectively (Fig. S1). The deleted regions of the mutants were verified by Sanger sequencing as well (Sanger *et al*., 1977).

Preparation of resting cells

Cells of *A. woodii* wild type, *Δfhs2*, *ΔfdhC* and *Δfhs2/fdhC* were grown on 20 mM fructose in 500 ml complex medium to late exponential growth phase (OD_{600} of 1.2 to 1.5) and then harvested by centrifugation (Avanti™J-25 and JA-10 Fixed-Angle Rotor; Beckman Coulter, Brea, CA, United States) at 7000 × g and 4°C for 10 min. The harvested cells were washed twice with 30 ml of buffer containing 50 mM imidazole (pH 7.0), 20 mM KCl, 20 mM $MgSO_4$, 4 mM DTE and 4 µM resazurin by centrifugation at 8500 rpm (5948 × g) and 4°C for 10 min (Avanti™J-25 and JA-25.50 Fixed-Angle Rotor; Beckman Coulter, Brea, CA, United States). Then, the cells were resuspended in 5 ml of buffer and kept in 16 ml Hungate tubes. All the steps were performed under strictly oxygen free conditions in an anoxic chamber (Coy Laboratory Products, Grass Lake, MI, United States) filled with N_2/H_2 (96%–98%/2%–4%; v/v). After taking out of the anoxic chamber, the headspace of Hungate tubes filled with resting

cells was changed to 100% N_2. The total protein concentration in the resting cells was measured using the method by (Schmidt *et al*., 1963).

Cell suspension experiments

The resting cells were filled into 115 ml serum flasks to a volume of 10 ml of imidazole buffer (50 mM imidazole, 20 mM KCl, 20 mM NaCl, 20 mM $MgSO_4$, 4 mM DTE, 4 μM resazurin, pH 7.0) and to a total protein concentration of 1 mg ml^{-1}. As substrate, either formate (4 mM or 350 mM) or 1 bar overpressure of $H_2 + CO_2$ (80%/20%; v/v) was added to the resting cells. The experiments were started with incubation at 30°C in water bath with shaking (230 rpm). 0.5 ml samples were taken at each time point for determination of formate and acetate.

Determination of H_2, formate and acetate

H_2 was determined by gas chromatography as described previously (Weghoff and Müller, 2016). The concentrations of formate and acetate were determined by high performance liquid chromatography (P680 HPLC Pump, ASI-100 Automated Sample Injector and Thermostatted Column Compartment TCC-100, Dionex, Sunnyvale, California, USA) with a HyperREZ XP Carbohydrate H^+ ion exchange column for sugar and acid separation (Thermo Fisher Scientific, Waltham, Massachusetts, USA) as described previously (Moon *et al*., 2019).

Acknowledgement

We are indebted to the European Research Council (ERC) for financial support under the European Union's Horizon 2020 research and innovation program (ACETOGENS, grant agreement no. 741791).

Conflict of interest

The authors declare that there is no conflict of interest.

References

Andreesen, J.R., and Ljungdahl, L.G. (1973) Formate dehydrogenase of *Clostridium thermoaceticum*: incorporation of selenium-75, and the effects of selenite, molybdate, and tungstate on the enzyme. *J Bacteriol* **116**: 867–873.

Balch, W.E., Schoberth, S., Tanner, R.S., and Wolfe, R.S. (1977) *Acetobacterium*, a new genus of hydrogen-oxidizing, carbon dioxide-reducing, anaerobic bacteria. *Int J Syst Bact* **27**: 355–361.

Bertsch, J., and Müller, V. (2015) CO metabolism in the acetogen *Acetobacterium woodii*. *Appl Environ Microbiol* **81**: 5949–5956.

Bertsch, J., Siemund, A.L., Kremp, F., and Müller, V. (2016) A novel route for ethanol oxidation in the acetogenic bacterium *Acetobacterium woodii*: the acetaldehyde/ethanol dehydrogenase pathway. *Environ Microbiol* **18**: 2913–2922.

Breznak, J.A., and Switzer, J.M. (1986) Acetate synthesis from H_2 plus CO_2 by termite gut microbes. *Appl Environ Microbiol* **52**: 623–630.

Buschhorn, H., Dürre, P., and Gottschalk, G. (1989) Production and utilization of ethanol by the homoacetogen *Acetobacterium woodii*. *Appl Environ Microbiol* **55**: 1835–1840.

Chabriere, E., Charon, M.H., Volbeda, A., Pieulle, L., Hatchikian, E.C., and Fontecilla-Camps, J.C. (1999) Crystal structures of the key anaerobic enzyme pyruvate:ferredoxin oxidoreductase, free and in complex with pyruvate. *Nat Struct Biol* **6**: 182–190.

Daniel, S.L., Hsu, T., Dean, S.I., and Drake, H.L. (1990) Characterization of the H_2-dependent and CO-dependent chemolithotrophic potentials of the acetogens *Clostridium thermoaceticum* and *Acetogenium kivui*. *J Bacteriol* **172**: 4464–4471.

Daniel, S.L., Keith, E.S., Yang, H.C., Lin, Y.S., and Drake, H.L. (1991) Utilization of methoxylated aromatic compounds by the acetogen *Clostridium thermoaceticum* - expression and specificity of the CO-dependent *O*-demethylating activity. *Biochem Biophys Res Commun* **180**: 416–422.

Deaton, J.C., Solomon, E.I., Watt, G.D., Wetherbee, P.J., and Durfor, C.N. (1987) Electron paramagnetic resonance studies of the tungsten-containing formate dehydrogenase from *Clostridium thermoaceticum*. *Biochem Biophys Res Commun* **149**: 424–430.

Dönig, J., and Müller, V. (2018) Alanine, a novel growth substrate for the acetogenic bacterium *Acetobacterium woodii*. *Appl Environ Microbiol* **84**: e02023–18.

Drake, H.L. (1994) Acetogenesis, acetogenic bacteria, and the acetyl-CoA pathway: past and current perspectives. In *Acetogenesis*, Drake, H.L. (ed). New York: Chapman and Hall, pp. 3–60.

Eichler, B., and Schink, B. (1984) Oxidation of primary aliphatic alcohols by *Acetobacterium carbinolicum* sp. nov., a homoacetogenic anaerobe. *Arch Microbiol* **140**: 147–152.

Falke, D., Schulz, K., Doberenz, C., Beyer, L., Lilie, H., Thiemer, B., and Sawers, R.G. (2010) Unexpected oligomeric structure of the FocA formate channel of *Escherichia coli*: a paradigm for the formate-nitrite transporter family of integral membrane proteins. *FEMS Microbiol Lett* **303**: 69–75.

Fontaine, F.E., Peterson, W.H., McCoy, E., Johnson, M.J., and Ritter, G.J. (1942) A new type of glucose fermentation by *Clostridium thermoaceticum*. *J Bacteriol* **43**: 701–715.

Genthner, B.R., and Bryant, M.P. (1982) Growth of *Eubacterium limosum* with carbon monoxide as the energy source. *Appl Environ Microbiol* **43**: 70–74.

Genthner, B.R.S., and Bryant, M.P. (1987) Additional characteristics of one-carbon-compound utilization by *Eubacterium limosum* and *Acetobacterium woodii*. *Appl Environ Microbiol* **53**: 471–476.

Heap, J.T., Pennington, O.J., Cartman, S.T., and Minton, N. P. (2009) A modular system for *Clostridium* shuttle plasmids. *J Microbiol Methods* **78**: 79–85.

Heise, R., Müller, V., and Gottschalk, G. (1989) Sodium dependence of acetate formation by the acetogenic bacterium *Acetobacterium woodii*. *J Bacteriol* **171**: 5473–5478.

Hess, V., Poehlein, A., Weghoff, M.C., Daniel, R., and Müller, V. (2014) A genome-guided analysis of energy conservation in the thermophilic, cytochrome-free acetogenic bacterium *Thermoanaerobacter kivui*. *BMC Genomics* **15**: 1139.

Hunger, D., Doberenz, C., and Sawers, R.G. (2014) Identification of key residues in the formate channel FocA that control import and export of formate. *Biol Chem* **395**: 813–825.

Kallen, R.G., and Jencks, W.P. (1966) The mechanism of the condensation of formaldehyde with tetrahydrofolic acid. *J Biol Chem* **241**: 5851–5863.

Kreft, J.U., and Schink, B. (1997) Specificity of O-demethylation in extracts of the homoacetogenic *Holophaga foetida* and demethylation kinetics measured by a coupled photometric assay. *Arch Microbiol* **167**: 363–368.

Kremp, F., and Müller, V. (2020) Methanol and methyl group conversion in acetogenic bacteria: biochemistry, physiology and application. *FEMS Microbiol Rev* **45**: fuaa040.

Kremp, F., Poehlein, A., Daniel, R., and Müller, V. (2018) Methanol metabolism in the acetogenic bacterium *Acetobacterium woodii*. *Environ Microbiol* **20**: 4369–4384.

Küsel, K., Dorsch, T., Acker, G., Stackebrandt, E., and Drake, H.L. (2000) *Clostridium scatologenes* strain SL1 isolated as an acetogenic bacterium from acidic sediments. *Int J Syst Evol Microbiol* **50**: 537–546.

Lechtenfeld, M., Heine, J., Sameith, J., Kremp, F., and Müller, V. (2018) Glycine betaine metabolism in the acetogenic bacterium *Acetobacterium woodii*. *Environ Microbiol* **20**: 4512–4525.

Leigh, J.A., Mayer, F., and Wolfe, R.S. (1981) *Acetogenium kivui*, a new thermophilic hydrogen-oxidizing, acetogenic bacterium. *Arch Microbiol* **129**: 275–280.

Lorowitz, W.H., and Bryant, M.P. (1984) *Peptostreptococcus productus* strain that grows rapidly with CO as the energy source. *Appl Environ Microbiol* **47**: 961–964.

Love, M.I., Huber, W., and Anders, S. (2014) Moderated estimation of fold change and dispersion for RNA-seq data with DESeq2. *Genome Biol* **15**: 550.

Lovell, C.R., Przybyla, A., and Ljungdahl, L.G. (1990) Primary structure of the thermostable formyltetrahydrofolate synthetase from *Clostridium thermoaceticum*. *Biochemistry* **29**: 5687–5694.

Luo, W., and Brouwer, C. (2013) Pathview: an R/Bioconductor package for pathway-based data integration and visualization. *Bioinformatics* **29**: 1830–1831.

Lynd, L.H., Kerby, R., and Zeikus, J.G. (1982) Carbon monoxide metabolism of the methylotrophic acidogen *Butyribacterium methylotrophicum*. *J Bacteriol* **149**: 255–263.

Matthies, D., Zhou, W., Klyszejko, A.L., Anselmi, C., Yildiz, O., Brandt, K., *et al*. (2014) High-resolution structure and mechanism of an F/V-hybrid rotor ring in a Na^+-coupled ATP synthase. *Nat Commun* **5**: 5286.

Mechichi, T., Labat, M., Woo, T.H., Thomas, P., Garcia, J.L., and Patel, B.K. (1998) *Eubacterium aggregans* sp. nov., a new homoacetogenic bacterium from olive mill wastewater treatment digestor. *Anaerobe* **4**: 283–291.

Moon, J., Henke, L., Merz, N., and Basen, M. (2019) A thermostable mannitol-1-phosphate dehydrogenase is required in mannitol metabolism of the thermophilic acetogenic bacterium *Thermoanaerobacter kivui*. *Environ Microbiol* **21**: 3728–3736.

Müller, V. (2003) Energy conservation in acetogenic bacteria. *Appl Environ Microbiol* **69**: 6345–6353.

Oswald, F., Stoll, I.K., Zwick, M., Herbig, S., Sauer, J., Boukis, N., and Neumann, A. (2018) Formic acid formation by *Clostridium ljungdahlii* at elevated pressures of carbon dioxide and hydrogen. *Front Bioeng Biotechnol* **6**: 6.

Peters, V., Janssen, P.H., and Conrad, R. (1999) Transient production of formate during chemolithotrophic growth of anaerobic microorganisms on hydrogen. *Curr Microbiol* **38**: 285–289.

Poehlein, A., Schmidt, S., Kaster, A.-K., Goenrich, M., Vollmers, J., Thürmer, A., *et al*. (2012) An ancient pathway combining carbon dioxide fixation with the generation and utilization of a sodium ion gradient for ATP synthesis. *PLoS One* **7**: e33439.

Radfar, R., Leaphart, A., Brewer, J.M., Minor, W., Odom, J.D., Dunlap, R.B., *et al*. (2000a) Cation binding and thermostability of FTHFS monovalent cation binding sites and thermostability of N10-formyltetrahydrofolate synthetase from *Moorella thermoacetica*. *Biochemistry* **39**: 14481–14486.

Radfar, R., Shin, R., Sheldrick, G.M., Minor, W., Lovell, C.R., Odom, J.D., *et al*. (2000b) The crystal structure of N10-formyltetrahydrofolate synthetase from M*oorella thermoacetica*. *Biochemistry* **39**: 3920–3926.

Ragsdale, S.W., and Pierce, E. (2008) Acetogenesis and the Wood-Ljungdahl pathway of CO_2 fixation. *Biochim Biophys Acta* **1784**: 1873–1898.

Sanger, F.S., Nickelen, F., and Coulson, A.R. (1977) DNA-sequencing with chain-terminating inhibitors. *Proc Natl Acad Sci U S A* **74**: 5463–5467.

Savage, M.D., Wu, Z.G., Daniel, S.L., Lundie, L.L., Jr., and Drake, H.L. (1987) Carbon monoxide-dependent chemolithotrophic growth of *Clostridium thermoautotrophicum*. *Appl Environ Microbiol* **53**: 1902–1906.

Schink, B. (1994) Diversity, ecology, and isolation of acetogenic bacteria. In *Acetogenesis*, Drake, H.L. (ed). New York: Chapman & Hall, pp. 197–235.

Schmidt, K., Liaaen-Jensen, S., and Schlegel, H.G. (1963) Die Carotinoide der *Thiorhodaceae*. *Arch Mikrobiol* **46**: 117–126.

Schoelmerich, M.C., Katsyv, A., Sung, W., Mijic, V., Wiechmann, A., Kottenhahn, P., *et al*. (2018) Regulation of lactate metabolism in the acetogenic bacterium *Acetobacterium woodii*. *Environ Microbiol* **20**: 4587–4595.

Schuchmann, K., and Müller, V. (2013) Direct and reversible hydrogenation of CO_2 to formate by a bacterial carbon dioxide reductase. *Science* **342**: 1382–1385.

Schuchmann, K., and Müller, V. (2014) Autotrophy at the thermodynamic limit of life: a model for energy conservation in acetogenic bacteria. *Nat Rev Microbiol* **12**: 809–821.

Schwarz, F.M., Schuchmann, K., and Müller, V. (2018) Hydrogenation of CO_2 at ambient pressure catalyzed by a highly active thermostable biocatalyst. *Biotechnol Biofuels* **11**: 237.

Simankova, M.V., Kotsyurbenko, O.R., Stackebrandt, E., Kostrikina, N.A., Lysenko, A.M., Osipov, G.A., and Nozhevnikova, A.N. (2000) *Acetobacterium tundrae* sp. nov., a new psychrophilic acetogenic bacterium from tundra soil. *Arch Microbiol* **174**: 440–447.

Song, Y., Lee, J.S., Shin, J., Lee, G.M., Jin, S., Kang, S., *et al*. (2020) Functional cooperation of the glycine synthase-reductase and Wood-Ljungdahl pathways for autotrophic growth of *Clostridium drakei*. *Proc Natl Acad Sci U S A* **117**: 7516–7523.

Tanner, R.S., Miller, L.M., and Yang, D. (1993) *Clostridium ljungdahlii* sp. nov., an acetogenic species in clostridial rRNA homology group-I. *Int J Syst Bact* **43**: 232–236.

Traunecker, J., Preuss, A., Diekert, G., and Preuss, A. (1991) Isolation and characterization of a methyl chloride utilizing, strictly anaerobic bacterium. *Arch Microbiol* **156**: 416–421.

Wang, S., Huang, H., Kahnt, J., and Thauer, R.K. (2013) A reversible electron-bifurcating ferredoxin- and NAD-dependent [FeFe]-hydrogenase (HydABC) in *Moorella thermoacetica*. *J Bacteriol* **195**: 1267–1275.

Weghoff, M.C., and Müller, V. (2016) CO metabolism in the thermophilic acetogen *Thermoanaerobacter kivui*. *Appl Environ Microbiol* **82**: 2312–2319.

Weghoff, M.C., Bertsch, J., and Müller, V. (2015) A novel mode of lactate metabolism in strictly anaerobic bacteria. *Environ Microbiol* **17**: 670–677.

Werner, H., Krasemann, C., Gorniak, W., Hermann, A., and Ungerechts, J. (1977) Susceptibility to thiamphenicol and chloramphenicol of anaerobic bacteria (author's transl). *Zentralbl Bakteriol Orig A* **237**: 358–371.

Westphal, L., Wiechmann, A., Baker, J., Minton, N.P., and Müller, V. (2018) The Rnf complex is an energy coupled transhydrogenase essential to reversibly link cellular NADH and ferredoxin pools in the acetogen *Acetobacterium woodii*. *J Bacteriol* **200**: e00357–18.

Wiechert, M., and Beitz, E. (2017) Mechanism of formate-nitrite transporters by dielectric shift of substrate acidity. *EMBO J* **36**: 949–958.

Wood, H.G., Ragsdale, S.W., and Pezacka, E. (1986) The acetyl-CoA pathway of autotrophic growth. *FEMS Microbiol Rev* **39**: 345–362.

Yamamoto, I., Saiki, T., Liu, S.M., and Ljungdahl, L.G. (1983) Purification and properties of NADP-dependent formate dehydrogenase from *Clostridium thermoaceticum*, a tungsten-selenium-iron protein. *J Biol Chem* **258**: 1826–1832.

Yishai, O., Lindner, S.N., Gonzalez de la Cruz, J., Tenenboim, H., and Bar-Even, A. (2016) The formate bio-economy. *Curr Opin Chem Biol* **35**: 1–9.

Yu, G., Wang, L.G., Han, Y., and He, Q.Y. (2012) clusterProfiler: an R package for comparing biological themes among gene clusters. *OMICS* **16**: 284–287.

Zelcbuch, L., Lindner, S.N., Zegman, Y., Vainberg Slutskin, I., Antonovsky, N., Gleizer, S., *et al*. (2016) Pyruvate formate-lyase enables efficient growth of *Escherichia coli* on acetate and formate. *Biochemistry* **55**: 2423–2426.

Zhu, A., Ibrahim, J.G., and Love, M.I. (2019) Heavy-tailed prior distributions for sequence count data: removing the noise and preserving large differences. *Bioinformatics* **35**: 2084–2092.

Supporting Information

Additional Supporting Information may be found in the online version of this article at the publisher's web-site:

Appendix S1: Supporting Information.